Journal of Power Sources 195 (2010) 1793–1798

Contents lists available at ScienceDirect

Journal of Power Sources

journal homepage: www.elsevier.com/locate/jpowsour

Fabrication and performance of membrane solid oxide fuel cells with $La_{0.75}Sr_{0.25}Cr_{0.5}Mn_{0.5}O_{3-\delta}$ impregnated anodes

Xingbao Zhu [a,*], Zhe Lü [a], Bo Wei [a], Kongfa Chen [a], Mingliang Liu [a], Xiqiang Huang [a], Wenhui Su [a,b]

[a] Center for Condensed Matter Science and Technology, Department of Physics, Harbin Institute of Technology, Harbin 150080, PR China
[b] International Center for Material Physics, Academia, Shenyang 110015, PR China

ARTICLE INFO

Article history:
Received 25 August 2009
Received in revised form 15 October 2009
Accepted 15 October 2009
Available online 23 October 2009

Keywords:
Solid oxide fuel cells
Perovskite oxide
LSCrM
Wet impregnation
Porous anode

ABSTRACT

$La_{0.75}Sr_{0.25}Cr_{0.5}Mn_{0.5}O_{3-\delta}$ (LSCrM)-impregnated anodes have been fabricated by infiltrating 70% porous yttria-stabilized zirconia (YSZ) matrixes with an LSCrM solution. In these anodes, LSCrM is a primary electronic conducive phase while the well-sintered YSZ provides an ionic-conducting pathway throughout the electrode. The maximum power densities of a single cell with YSZ + 35 wt.% LSCrM composite anode reach 567 and 561 mW cm^{-2} at 850 °C in dry H_2 and CH_4, respectively. Further, Ag and Ni are added via nitrate impregnating method for improving electronic conductivity and catalytic activity. With the addition of 6 wt.% Ni and 2 wt.% Ag to the YSZ + 32 wt.% LSCrM composite anode, the maximum power densities at 850 °C increase to 1302 mW cm^{-2} in dry H_2 and 769 mW cm^{-2} in dry CH_4. No carbon deposition is detected in the tested anodes, even with the presence of Ni.

1. Introduction

There are several advantages for solid oxide fuel cells (SOFCs) such as high efficiency, less pollution, fuel flexibility and higher tolerance to impurities in the fuel. The commonly used fuel for SOFCs is pure hydrogen. To facilitate the commercialization of SOFCs, it is needed to substitute pure hydrogen with economical hydrocarbon fuels such as methane. The traditional anode material for SOFC with YSZ (YSZ: yttria-stabilized zirconia) electrolyte is Ni/YSZ cermets which provide high performance with hydrogen fuel, but undergo carbon deposition in hydrocarbon fuels due to the tendency of Ni to catalyze C–C bond formation [1,2]. Recently, great efforts have been paid on the development of new anode materials using hydrocarbon fuels directly. Ni-free oxides such as ceria [3], titanate [4] and some other perovskite oxides [5,6] have received increasing attention. Tao et al. [7,8] reported a redox stable $(La,Sr)(Cr,Mn)O_{3-\delta}$ anode which can effectively inhibit carbon deposition, but does not have adequate electrocatalytic activity for fuel oxidation because of its low ionic and electronic conductivity [9,10]. To modify the perovskite anode, some materials with higher ionic, electronic conductivities and better catalytic activity such as $(Sm,Ce)O_{2-\delta}$ (SDC) [11], $(Gd,Ce)O_{2-\delta}$ (GDC) [12], Cu [13,14], Ni [15] and Pd [16,17] have been introduced into LSCrM anodes. The introduction methods could be classified as mechanical mixing and wet impregnation. The advantages of the wet impregnation technique have been confirmed by the previous work [18,19], e.g. simple process, low sintering temperature, easily achieving fine grain size and stable sintering behavior.

In the present study, $La_{0.75}Sr_{0.25}Cr_{0.5}Mn_{0.5}O_{3-\delta}$ (LSCrM) impregnated anodes were prepared by infiltrating porous YSZ matrix with LSCrM nitrate solutions. In these anodes, YSZ acted as a backbone and provided an ionic-conducting pathway throughout the electrode facilitating the fuel oxidation. Metal Ag and Ni were also introduced via an impregnation method to improve the electronic conductivity and catalytic activity. The cell with this ceramic anode exhibited desirable performance using either hydrogen or methane as the reductant.

2. Experimental methods

2.1. Cell fabrication

The raw powders of NiO (Inco, Canada), YSZ (TZ-8Y, Tosoh, Japan) and tapioca pore former were thoroughly mixed in a weight ratio of 6:5:4. The mixture was pressed into a pellet of 13 mm in diameter and 0.5 mm in thickness, and then fired at 1000 °C for 2 h. YSZ electrolyte film was coated on one surface of the prefired pellet by slurry spin coating technique and sintered at 1400 °C for 4 h as described elsewhere [20]. After being reduced in hydrogen, the bilayer was dipped in a dilute nitric acid for 12 h to soak out the Ni. Then, a porous YSZ anode layer coated with dense YSZ film was obtained, and its porosity was as high as about 70%. LSCrM was then

* Corresponding author. Tel.: +86 451 86418420; fax: +86 451 86418420.
E-mail address: zhuxingbao008@163.com (X. Zhu).

0378-7753/$ – see front matter © 2009 Elsevier B.V. All rights reserved.
doi:10.1016/j.jpowsour.2009.10.042

added into the porous YSZ layer by an ion impregnation technique to form an YSZ/LSCrM composite anode.

The impregnating solution was prepared by the following steps: stoichiometric amounts of prefired La_2O_3 were dissolved into dilute nitric acid to form nitrate then stoichiometric amounts of $Cr(NO_3)_3{\cdot}9H_2O$ (99%), $Sr(NO_3)_2$ (99.5%) and $Mn(NO_3)_2$ (50%) were added to form a mixed nitrate solution with the required metal ions stoichiometry; finally, urea as complexing and dispersing agent [21] was added at the urea/metal molar ratio of 2:1 to prepare an LSCrM solution. The LSCrM solution was dipped on the surface of the YSZ matrix, and it infiltrated into the pores of the porous YSZ layer under capillary action, dried and heated at 300 °C. This impregnation process was repeated until a desired loading of LSCrM was achieved. After impregnation of LSCrM, cathode ($La_{0.8}Sr_{0.2}MnO_{3-\delta}$) slurry [15,22] was coated onto the electrolyte film, and the three-layer was co-sintered at 1100 °C for 2 h in air to produce well-sintered cathode layer and the perovskite phase of the LSCrM. Next, metal Ni and Ag were loaded into some LSCrM/YSZ anodes as catalyst and electronic conductive phase by addition of aqueous solutions of the nitrate salts and heating in air to 850 °C. During the process of the metal impregnation, cathode was sealed with wax. For comparison, a cell with Ni impregnated YSZ anode was prepared. Before addition of Ni, cathode was coated and sintered at 1100 °C for 2 h. The porous anode layer was then impregnated with $Ni(NO_3)_2$ solution. After the impregnation of Ni, the cell was fired at 850 °C for 1 h. In this study, $La_{0.8}Sr_{0.2}MnO_{3-\delta}$ cathodes were all modified with SDC nano-particles by impregnating $Ce_{0.8}Sm_{0.2}(NO_3)_x$ solution [23].

2.2. Characterization

Differential thermal analysis (DTA) and thermal gravity analysis (TGA) data for a YSZ matrix impregnated with LSCrM solution and dried at room temperature were obtained from a thermal analyzer (TA SDT2960, USA) in air. The data were collected from room temperature to 1000 °C at a rate of 10 °C min^{-1}. Perovskite phase of the impregnated LSCrM was characterized by X-ray diffraction (XRD, Rigaku D/max rB, Japan), using Cu Kα radiation (λ = 0.15418 nm).

A four-probe method was used to test the fuel cells. The anode-supported single cell was sealed on one end of an alumina tube with silver paste (DAD-87, Shanghai Research Institute of Synthetic Resins), in which dry H_2 or CH_4 was used as the fuel at the anode and stationary air as the oxidant at the cathode. The fuels were controlled by a mass flow controller (D08-4D/2M, Seven Star Huachuang). During the cell test, the flow rate was fixed at 100 sccm for H_2 and 70 sccm for CH_4, respectively. The electrochemical measurements on these cells were performed over the temperature range 700–850 °C by means of impedance spectroscopy and *I–V* curve measurement using an SI 1287 electrochemical interface and SI 1260 impedance analyzer (Solartron Instruments, Hampshire, UK). The anode microstructure was revealed by scanning electron microscope (SEM, Hitachi S-4800, Japan). After cell operation for about 2 h in CH_4, the element microanalysis of both Ni impregnated and Ni/Ag/LSCrM co-impregnated anodes was carried out by energy dispersive X-ray (EDX, Horiba EMAX) spectrometer equipped with the Hitachi 4800.

3. Results and discussion

3.1. Thermal analysis

Fig. 1 shows the DTA and TGA curves for a porous YSZ matrix that was impregnated with LSCrM solution and dried at room temperature. The change at 100 °C for the curves of DTA and TGA is attributed to water evaporation. The major decomposition of the

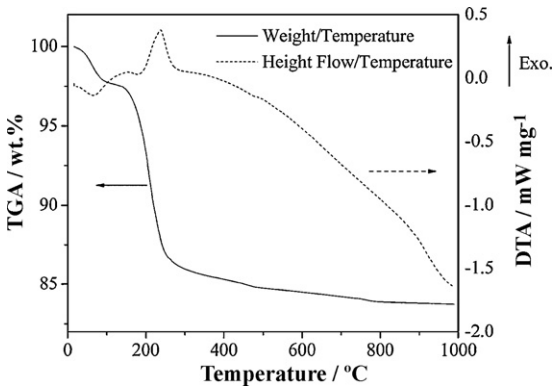

Fig. 1. Decomposition behavior of the LSCrM solution.

LSCrM precursor occurred in the temperature range of 150–300 °C, giving rise to a sharp exothermic peak in the DTA curve around 250 °C. The weight loss was 11.37% corresponding to decomposition of nitrate ions and urea. As described in previous studies [24,25], the temperature for the decomposition of $Cr(NO_3)_3$ and $Mn(NO_3)_2$ to Cr_2O_3 and MnO_2, respectively, was lower than 200 °C, for $La(NO_3)_3$ and $Sr(NO_3)_2$ the temperatures were about 600 and 700 °C, respectively. The temperature for sharp decomposition of urea was 230 °C [26], and the introduction of urea may reduce the decomposition temperature of these nitrate salts [21].

In this paper, the porous YSZ matrix after one impregnation of the LSCrM solution was fired at 300 °C that assured the decomposition of $Cr(NO_3)_3$, $Mn(NO_3)_2$ and urea. But the higher decomposition temperature produced the fired anode with undecomposed $La(NO_3)_3$ and $Sr(NO_3)_2$ that may dissolve in the LSCrM solution in the next impregnation process. Fortunately, it did not change the required metal ions stoichiometry in this impregnated anode because the LSCrM solution was dipped on the surface of the YSZ matrix and dried in situ, so the La and Sr ions did not loss. The heat treatment process facilitates the decomposition of the nitrate. But this temperature (300 °C) is not high enough to produce the LSCrM single-phase.

3.2. Phase formation

A 30 wt.% LSCrM-impregnated YSZ matrix sintered at 1100 °C for 2 h was characterized by XRD (Fig. 2). The characteristic X-ray peaks in Fig. 2 indicate that the perovskite phase of the LSCrM formed as the decomposition product of the nitrate precursor solution. No additional diffraction peaks were found in this simple indicating no reaction between LSCrM and YSZ. It also demonstrated that the

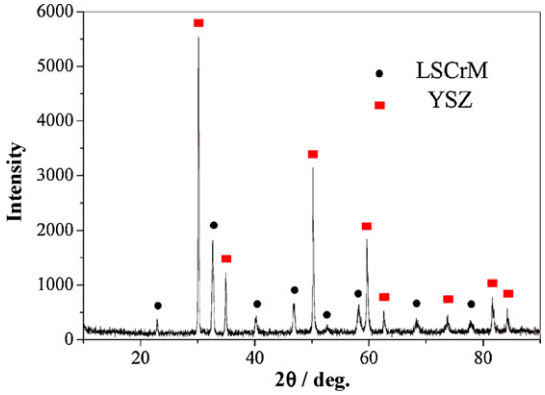

Fig. 2. An XRD pattern of a porous YSZ matrix impregnated with 30 wt.% LSCrM after sintering at 1000 °C for 2 h.

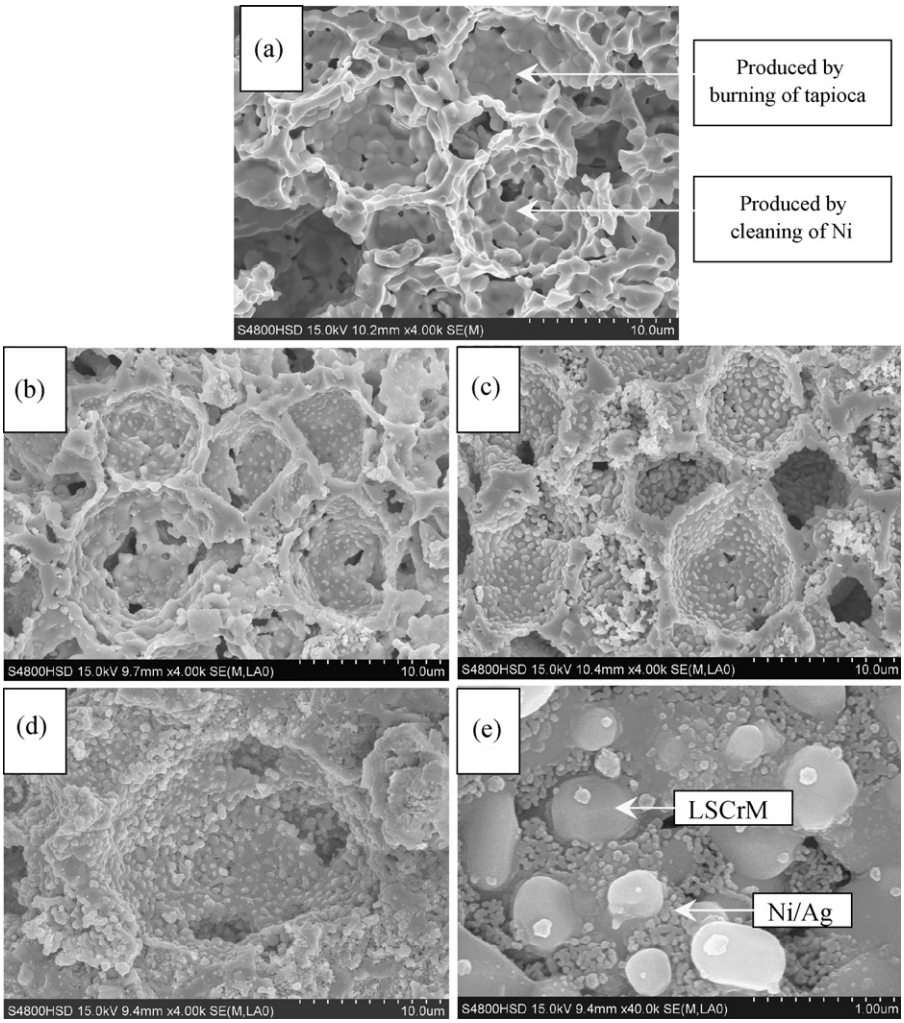

Fig. 3. SEM micrographs of the cross-sections of: (a) pure YSZ anode backbone; (b) ~5 wt.% LSCrM-impregnated YSZ anode; (c) ~35 wt.% LSCrM-impregnated YSZ anode; (d and e) LSCrM/Ni/Ag (~32/6/2 wt.%) impregnated YSZ anode.

undecomposed $La(NO_3)_3$ and $Sr(NO_3)_2$ in impregnation process did not influence the formation of the LSCrM.

3.3. Anode microstructure

Fig. 3(a) presents a porous YSZ anode backbone as the matrix prior to impregnation. The large, spherical pores with smooth inner surfaces resulted from the burning of tapioca, while the smaller pores, its inner surfaces covered with tiny "hills and valleys", were due to the cleaning of Ni. When 5 wt.% LSCrM was loaded, the LSCrM particles (~0.5 μm) were observed to cover the inner surface of the backbone and appeared to be discrete to each other, as shown in Fig. 3(b). It seems that the small LSCrM particles preferred to deposit on the boundaries of YSZ grains where low surface tension and surface energy can be achieved. At the loading of 35 wt.%, the LSCrM particles growed to about 1 μm and formed a connected network over the YSZ backbone in some little pores, as shown in Fig. 3(c). In Ni/Ag-impregnated LSCrM/YSZ anode (Fig. 3(d) and (e)), the Ni/Ag particles with a grain size of 100 nm were dispersed on the interfaces of LSCrM/YSZ grains and can act as a connector between LSCrM particles. No obvious differences in microstructure were noticed between Ni and Ag. These fine particles also can effectively expand the three phase boundary (TPB). Carbon depositions were not observed on these LSCrM-based anodes after operating with CH_4 fuel.

As indicated in Fig. 4, the elements were uniformly distributed inside the impregnated anode. The uniform distribution of the elements inside the porous YSZ matrix demonstrates that impregnation is an effective method for introducing active material into the electrodes of SOFCs.

3.4. Electrochemical performance

Fig. 5 shows the voltage and power density as a function of current density at 850 °C with dry H_2 and dry CH_4 as fuels for three single cells (cell-1, cell-2 and cell-3: cell-1 is denoted as the cell with 5 wt.% LSCrM-impregnated YSZ anode; cell-2 with 35 wt.% LSCrM-impregnated YSZ anode and cell-3 with 32 wt.% LSCrM + 6 wt.% Ni + 2 wt.% Ag-impregnated YSZ anode). Cathodes and electrolytes were all the same for them. The three cells exhibited open-circuit voltages (OCVs) of over 1.0 V measured at 850 °C, indicating the YSZ films are pinhole-free and gas-tight. The cell-3 exhibited the lowest OCVs just because of the multiple-sintering for YSZ film during impregnation process. *I–V* relationships were nearly linear. The maximum power densities of the cell-1 with 5 wt.% LSCrM-impregnated YSZ anode at 850 °C were 37 and 18 mW cm^{-2} in dry H_2 and CH_4, respectively. With the LSCrM loading level increased to 35 wt.%, the maximum power densities of the cell-2 increased substantially to 567 and 561 mW cm^{-2} at 850 °C in H_2 and CH_4, respectively, which are 15 and 32 times higher than that of cell-1.

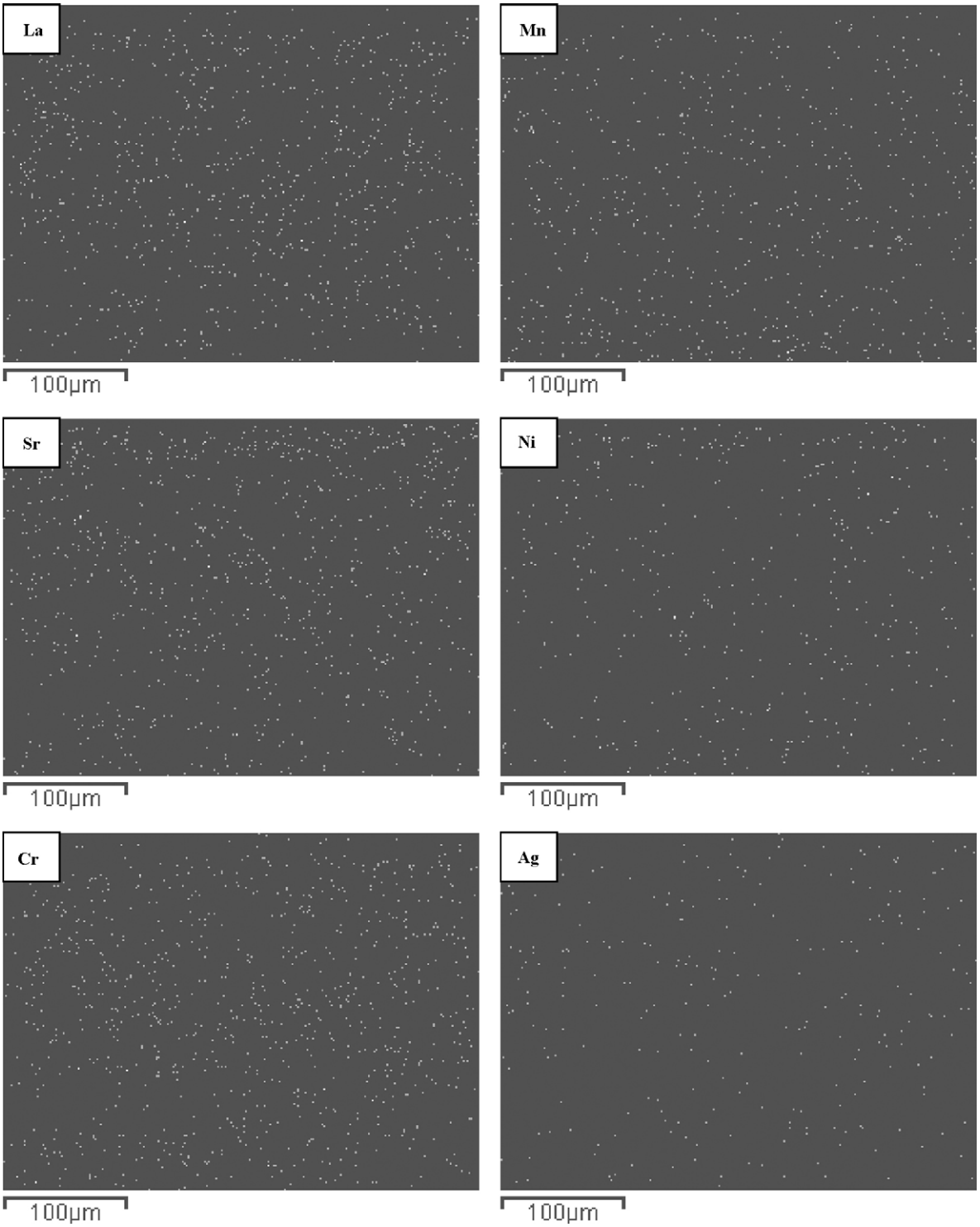

Fig. 4. The distribution of elements content (La, Sr, Cr, Mn, Ni and Ag) in the cross-section of the LSCrM/Ni/Ag (~32/6/2 wt.%) impregnated YSZ anode.

After the metal Ni and Ag were added, the maximum power densities of the cell-3 reached 1302 and 769 mW cm^{-2} using dry H_2 and CH_4 as fuels, respectively, which are 2.3 and 1.4 times higher than that of cell-2.

The testing results showed that the introduction of Ni and Ag into LSCrM-impregnated YSZ anode could significantly improve the cell performance. In order to determine the main factor of improving cell performance, the cell-4 (cell-4: a cell with 32 wt.% LSCrM and 6 wt.% Ni impregnated YSZ anode) was fabricated and tested under the same testing conditions. Without Ag, the cell performances at 850 °C were 1210 and 693 mW cm^{-2} in H_2 and CH_4, respectively, slightly lower than those of cell-3 (Fig. 6). It demonstrated that Ni played a key role for enhanced anode performance. In these LSCrM-based anodes, LSCrM should be a primary electronic conducive phase and electrocatalyst for direct oxidations of H_2 and CH_4. In order to check the effect of the LSCrM, a cell with 30 wt. % Ni impregnated YSZ anode was fabricated through the same preparation process and named as cell-5. As shown in Fig. 6, the values of the maximum power density of the cell-5 were 813 and 481 mW cm^{-2} in H_2 and CH_4, respectively, much lower than those

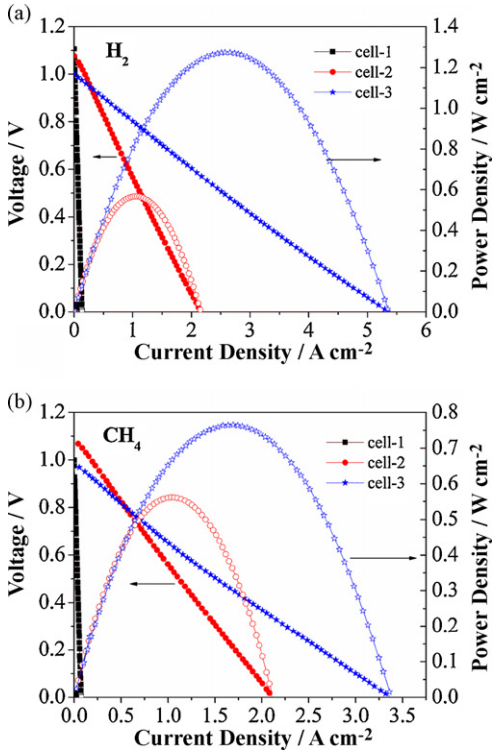

Fig. 5. *I–V* curves in (a) dry H_2 and (b) CH_4 at 850 °C for SOFCs with YSZ anodes impregnated with: (■) 5 wt.% LSCrM, (●) 35 wt.% LSCrM, (★) 32 wt.% LSCrM + 6 wt.% Ni + 2 wt.% Ag. The open symbols indicate the power densities.

of cell-3. And a clear polarization phenomenon was detected in their *I–V* curves. Short-term testing for cell-3 and cell-5 in CH_4 with a fixed current density was shown in Fig. 7. After 1 h the voltage loss was invisible for cell-3, but it could not be ignored for cell-5. Energy dispersive X-ray (EDX) analysis of the LSCrM/Ni/Ag-impregnated

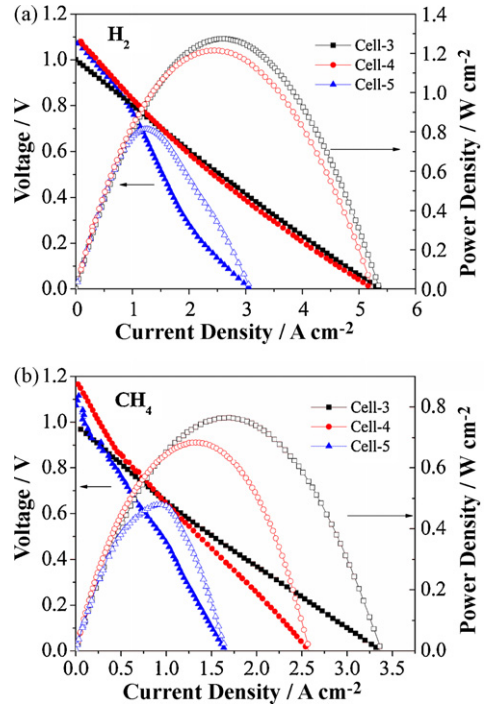

Fig. 6. *I–V* curves in (a) dry H_2 and (b) CH_4 at 850 °C for cell-3, cell-4 and cell-5. The open symbols indicate the power densities.

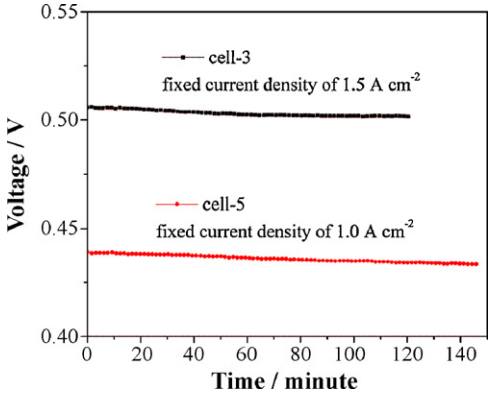

Fig. 7. The variation with time of the cell voltage for cell-3 and cell-5 in dry CH_4 at 850 °C. The current density was fixed at 1.5 A cm^{-2} for cell-3 and 1.0 A cm^{-2} for cell-5, respectively.

anode (Fig. 8) showed no detectable carbon deposition after cell operation for about 2 h in CH_4 near the maximum power point current density (1.5 A cm^{-2}). However, obvious carbon deposition was presented in Fig. 8 for only Ni impregnated anode after cell operation for >2 h in CH_4 near the maximum power point current density (1.0 A cm^{-2}). To confirm the properties of stability and carbon formation resistant for LSCrM-based anodes, long-term testing needs to be done further in the future.

The impedance spectra of the three cells are shown in Fig. 9(a) and (b). All the data were obtained at 850 °C in dry H_2 and CH_4 under open-circuit conditions. The total resistance can be divided into ohmic resistance and electrode polarization resistance. The high-frequency intercept of the impedance spectra corresponds to the cell ohmic resistance including electrolyte resistance of oxygen-ion conduction, electrodes' ohmic resistance and contact resistances of the interfaces. The high- and low-frequency depressed arcs are due to different electrode polarization processes [27]. When 5 wt.% LSCrM was impregnated into YSZ anode, the ohmic resistances for cell-1 were 4.76 and 4.93 Ω cm^2 at 850 °C in dry H_2 and CH_4, respectively. The large ohmic resistance means that most isolated LSCrM particles in the pores of YSZ matrix cannot work as effective anode sites, only the ones near surface contacting with current collector can work well. When the LSCrM loading increased to 35 wt.%, the corresponding ohmic resistances decreased down to 0.16 and 0.17 Ω cm^2. This is reasonable considering that LSCrM is the electronic conducive phase in these LSCrM-impregnated YSZ anodes. However, LSCrM is a predominant p-type conductor with the conductivity of 38 S cm^{-1} at 900 °C at the oxygen partial pressure above 10^{-10} atm and is essentially $p(O_2)$-independent [19,28]. The electronic conductivity of the LSCrM becomes much lower, e.g. 1.5 S cm^{-1} at 900 °C in 5% H_2, in the reducing atmosphere [14,29]. For this reason, metal Ag and Ni as electronic conductive phase and

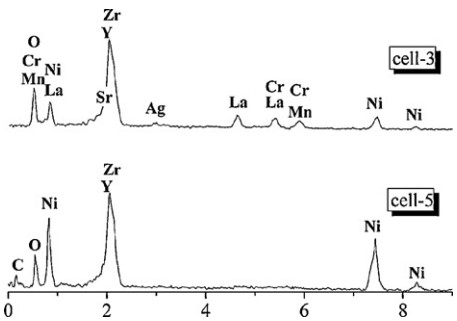

Fig. 8. EDX analysis of Ni/Ag/LSCrM or Ni impregnated YSZ anode after cell operation in dry CH_4 for about 2 h at 850 °C near the maximum power point current densities.

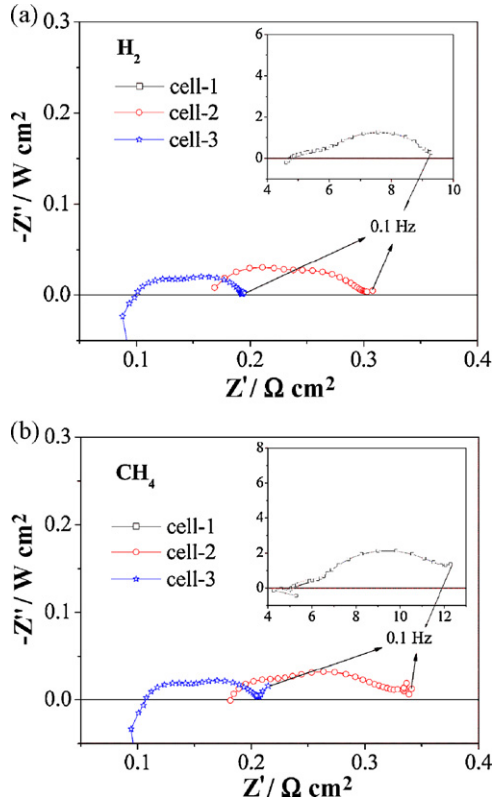

Fig. 9. Impedance spectra in (a) dry H_2 and (b) CH_4 at 850 °C for SOFCs with porous YSZ anodes impregnated with: (□) 5 wt.% LSCrM, (◯) 35 wt.% LSCrM, (☆) 32 wt.% LSCrM + 6 wt.% Ni + 2 wt.% Ag.

catalysts were added. After the introduction of Ni (6 wt.%) and Ag (2 wt.%), the ohmic resistance of the cell-3 decreased to 0.09 Ω cm^2 either in H_2 or CH_4 condition, in which the least electrode polarization resistance was also achieved, as shown in Fig. 9.

As clearly shown, the porous anode structure and wet impregnation technology lead to a significantly improvement in anode performance. However, the amount, morphology and spatial distribution of impregnated particles all influence the performance of the composite anode, which need a further study in the future.

4. Conclusion

The results of this study show that addition of LSCrM to a porous YSZ backbone via impregnation can produce an LSCrM anode with high performance indicating microstructure is very critical. The cell, with 32 wt.% LSCrM + 6 wt.% Ni + 2 wt.% Ag impregnated YSZ anode, YSZ electrolyte and SDC-impregnated LSM cathode, exhibited the best performance of 1302 and 769 mW cm^{-2} when H_2 and CH_4 were used as fuels, respectively. Carbon deposition was not detected in these LSCrM anodes with and without Ni.

Acknowledgements

The authors thank the Ministry of Science and Technology of China (contract no. 2007AA05Z139) for its financial support.

References

[1] H.P. He, J.M. Hill, Appl. Catal. A: Gen. 317 (2007) 284–292.
[2] B.C.H. Steele, I. Kelly, H. Middleton, R. Rudkin, Solid State Ionics 28 (1988) 1547–1552.
[3] Z.F. Zhou, R. Kumar, S.T. Thakur, L.R. Rudnick, H. Schobert, S.N. Lvov, J. Power Sources 171 (2007) 856–860.
[4] X.L. Huang, H.L. Zhao, W.H. Qiu, W.J. Wu, X. Li, Energ. Convers. Manage. 48 (2007) 1678–1682.
[5] J.W. Fergus, Solid State Ionics 177 (2006) 1529–1541.
[6] Y.H. Huang, R.I. Dass, Z.L. Xing, J.B. Goodenough, Science 312 (2006) 254–257.
[7] S.W. Tao, J.T.S. Irvine, Nat. Mater. 2 (2003) 320–325.
[8] S.W. Tao, J.T.S. Irvine, S.M. Plint, J. Phys. Chem. B 110 (2006) 21771–21776.
[9] V.V. Kharton, E.V. Tsipis, I.P. Marozau, A.P. Frade, J.T.S. Irvine, Solid State Ionics 178 (2007) 101–113.
[10] E.S. Raj, J.A. Kilner, J.T.S. Irvine, Solid State Ionics 177 (2006) 1747–1752.
[11] J. Peña-Martínez, D. Marrero-López, D. Pérez-Coll, J.C. Ruiz-Morales, P. Núñez, Electrochim. Acta 52 (2007) 2950–2958.
[12] X.J. Chen, Q.L. Liu, S.H. Chan, N.P. Brandon, K.A. Khor, Electrochem. Commun. 9 (2007) 767–772.
[13] X.F. Ye, S.R. Wang, Z.R. Wang, Q. Hu, X.F. Sun, T.L. Wen, Z.Y. Wen, J. Power Sources 183 (2008) 512–517.
[14] J. wan, J.H. Zhu, J.B. Goodenough, Solid State Ionics 177 (2006) 1211–1217.
[15] X.B. Zhu, Z. Lü, B. Wei, K.F. Chen, M.L. Liu, X.Q. Huang, W.H. Su, J. Power Sources 190 (2009) 326–330.
[16] G. Kim, G. Corre, J.T.S. Irvine, J.M. Vohs, R.J. Gorte, Electrochem. Solid-State Lett. 11 (2008) B16–B19.
[17] G. Kim, S. Lee, J.Y. Shen, G. Corre, J.T.S. Irvine, J.M. Vohs, R.J. Gorte, Electrochem. Solid-State Lett. 12 (2009) B48–B52.
[18] S.P. Jiang, Mater. Sci. Eng. A 418 (2006) 199–210.
[19] J.H. Qiao, K.N. Sun, N.Q. Zhang, B. Sun, J.R. Kong, D.R. Zhou, J. Power Sources 169 (2007) 253–258.
[20] K.F. Chen, Z. Lü, N. Ai, X.Q. Huang, Y.H. Zhang, X.S. Xin, R.B.W.H.S. Zhu, J. Power Sources 160 (2006) 436–438.
[21] S.K. Jung, C. Lu, H.P. He, K.Y. Ahn, R.J. Core, J.M. Vohs, J. Power Sources 154 (2006) 42–50.
[22] X.J. Chen, Q.L. Liu, K.A. Khor, S.H. Chan, J. Power Sources 165 (2007) 34–40.
[23] M.L. Liu, Z. Lü, B. Wei, X.Q. Huang, K.F. Chen, W.H. Su, Electrochim. Acta 54 (2009) 4726–4730.
[24] T. Cseri, S. Békássy, G. Kenessey, G. Liptay, F. Figueras, Thermochim. Acta 288 (1996) 137–1574.
[25] R. Karita, H. Kusaba, K. Sasaki, Y. Teraoka, Catal. Today 126 (2007) 471–475.
[26] P.M. Schaber, J. Colson, S. Higgins, D. Thielen, B. Anspach, J. Brauer, Thermochim. Acta 424 (2004) 131–142.
[27] X.C. Lu, J.H. Zhu, J. Power Sources 165 (2007) 678–684.
[28] X.C. Lu, J.H. Zhu, Solid State Ionics 178 (2007) 1467–1475.
[29] S.M. Plint, P.A. Connor, S.W. Tao, J.T.S. Irvine, Solid State Ionics 177 (2006) 2005–2008.